


 Cite this: *Chem. Commun.*, 2021, 57, 11629

 Received 31st August 2021,
 Accepted 12th October 2021

DOI: 10.1039/d1cc04863e

rsc.li/chemcomm

Enhanced syngas production from CO₂ photoreduction over CoPd alloy modified NiAl-LDH under visible light†

 Lan Yang,^{‡,a} Lei Li,^{‡,a} Pengfei Xia,^a Huiyi Li,^a Jingjing Yang,^a Xiaohong Li,^a Xiaodi Zeng,^a Xiaodong Zhang,^{id} Chong Xiao^{id}*^{ab} and Yi Xie^{id}^{ab}

We reported the modification of a NiAl-layered double hydroxide (LDH) by loading well-dispersed CoPd alloys through a NaBH₄ reduction method. The modified NiAl-LDH achieved 14.5-fold and 2.1-fold improvements of the H₂ and CO evolution rates and an applicable ratio of H₂/CO (nearly 1:1) under visible light ($\lambda > 420$ nm). This study revealed the potential of alloys to adjust the H₂/CO ratio and enhance syngas production for LDHs for the first time.

Converting CO₂ to valuable products by photoreduction is a potential way to solve the problems of fossil fuels depletion and environmental pollution. Among them, syngas, comprised of CO and H₂, is an extremely worthy product for its role as a feedstock in the production of liquid fuels by industrial technologies.¹ However, for practical applications, one important requirement for syngas is the appropriate ratio of H₂/CO. For example, in oxo synthesis and the production of dimethyl ether, a ratio of 1:1 is required.^{2,3} Thus, designing photocatalysts to produce syngas with applicable ratios is essential.

Several photocatalysts such as TiO₂,⁴ SrTiO₃,⁵ Co-ZIF-9,⁶ and layered double hydroxides (LDHs)^{7–9} have been reported for the synthesis of syngas from photocatalytic CO₂ reduction. Among these, LDHs have attracted extensive attention,^{10,11} due to their low cost, and tunable bandgap caused by adjustable types and amounts of cations.¹² LDHs are formed by orderly arranged two-dimensional laminates and negatively charged anions in the interlayer. Wang⁹ reported syngas production using a CoAl LDH and further tuned the ratio of H₂/CO by loading different amounts of Pd nanoparticles. However, the cost of Pd limited its application. Besides, previous reports of LDHs for producing syngas focused on regulation of the ratio, while the

simultaneous promotion of H₂ and CO evolution rates was rarely fulfilled.^{7,9} The modification of LDHs to produce photocatalysts with enhanced yields of H₂ and CO simultaneously and promise an applicable ratio remains a challenge. Bimetal alloys such as CuPd¹³ and AuPd¹⁴ present different lattice structures and active sites compared with pure metals, and have been reported to improve the activity and selectivity of photocatalysts. Thus, loading alloys of Pd and another non-precious metal onto LDHs may solve the challenge.

Herein, taking NiAl-LDH as a platform, we synthesized Pd nanoparticle loaded NiAl-LDH (NiAl-LDH-Pd) and CoPd alloy loaded NiAl-LDH (NiAl-LDH-CoPd), respectively, to deeply evaluate the influence of alloys on photocatalytic CO₂ reduction performance and their potential for converting CO₂ into syngas. Tests of charge kinetics reveal that the loading of the alloy facilitates the separation and transfer of charge carriers, which may be due to the more appropriate Schottky barrier height in NiAl-LDH-CoPd.¹⁵ Also, DFT calculations demonstrate that the active sites for CO₂ photoreduction and H₂ evolution are both optimized. Thus, under visible light ($\lambda > 420$ nm), the H₂ and CO evolution rates of NiAl-LDH-CoPd were 14.5 and 2.1 times higher than those of NiAl-LDH, and 3.3 and 5.6 times higher than those of NiAl-LDH-Pd. Furthermore, the productivities of H₂ and CO achieve a ratio close to 1:1, which meets the practical ratio requirement.

The NiAl-LDH was prepared by referring to a previous report.¹⁶ The X-ray diffraction (XRD) patterns showed (Fig. S1, ESI†) the typical diffraction peaks of NiAl-LDH (JCPDS No. 015-0087).¹⁷ Besides, the broad peaks indicated its poor crystallinity. Subsequently, Pd nanoparticles and CoPd alloy nanoparticles were grown on the NiAl-LDH *in situ* by the reduction of NaBH₄.¹⁸ The obtained NiAl-LDH-Pd and NiAl-LDH-CoPd displayed the same XRD patterns as NiAl-LDH (Fig. S1, ESI†). Neither the diffraction peaks of Pd nor CoPd appeared. This may be ascribed to the small size and high dispersion of the Pd and CoPd nanoparticles in the heterostructure photocatalysts.^{9,18} The results of inductively coupled plasma atomic emission spectroscopy (ICP-AES) indicated the same weight percentages of Pd and Co + Pd in the respective composites

^a Hefei National Laboratory for Physical Sciences at the Microscale, CAS Center for Excellence in Nanoscience, University of Science and Technology of China, Hefei, Anhui, 230026, P. R. China. E-mail: cxiao@ustc.edu.cn

^b Institute of Energy, Hefei Comprehensive National Science Center, Hefei, Anhui, 230031, P. R. China

† Electronic supplementary information (ESI) available: Details of experimental methods and additional figures and tables. See DOI: 10.1039/d1cc04863e

‡ These authors contributed equally to this work.

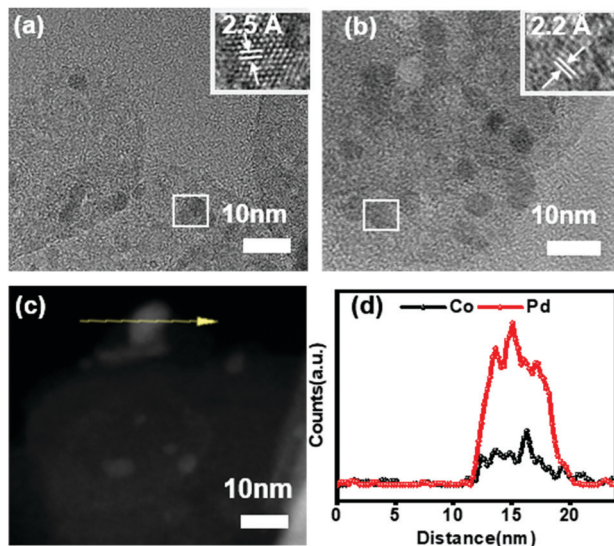


Fig. 1 HRTEM images of (a) NiAl-LDH-Pd and (b) NiAl-LDH-CoPd; the insets of (a and b) show the images taken from the regions marked by the boxes corresponding to Pd and CoPd particles respectively; (c) HAADF-STEM image of NiAl-LDH-CoPd; (d) EDS line mapping profiles of CoPd particles along the directions marked by the yellow lines in (c).

(Table S1, ESI[†]), which excludes the influence of the metal loading amounts on photocatalytic activity. Fig. S2 (ESI[†]) and Fig. S3 (ESI[†]) display the scanning electron microscopy (SEM) and transmission electron microscopy (TEM) images of photocatalysts. NiAl-LDH showed a flat nanosheet shape with an average width smaller than 200 nm and a thickness of around 5 nm. The Pd and CoPd nanoparticles both showed evenly deposition and diameters ranging from 3–8 nm, and the averages diameter were 5.4 nm and 5.3 nm, respectively. The NiAl-LDHs maintained their original morphology after loading of the Pd and CoPd nanoparticles. High-resolution transmission electron microscopy (HRTEM) analysis (Fig. 1a and b) was conducted to verify the formation of the alloys. In NiAl-LDH-Pd (Fig. 1a), NiAl-LDH showed no obvious lattice fringes due to the poor crystallinity, which was in agreement with the XRD results. The spacing of the continuous lattice fringes in the Pd nanoparticles is 2.5 Å, which can be ascribed to the (200) planes of fcc-Pd. As for NiAl-LDH-CoPd (Fig. 1b), the CoPd nanoparticles displayed lattice fringes with a spacing of 2.2 Å, which was close to the interplanar spacing of the fcc-Pd (111) planes (2.23 Å) and is the same as reported CoPd alloys.¹⁹ Further, high-angle annular dark-field scanning TEM (HAADF-STEM) images (Fig. 1c) and the corresponding energy-dispersive X-ray spectroscopy (EDS) line scans (Fig. 1d) of the CoPd nanoparticle were collected, the signals of Co and Pd appeared at the nearly same position, indicating the formation of CoPd alloys.¹³ The results from the X-ray photoelectron spectroscopy (XPS) analysis showed that the Pd exists in the form of Pd(0) and Pd(II) species in both NiAl-LDH-Pd (Fig. S7a, ESI[†]) and NiAl-LDH-CoPd (Fig. S7b, ESI[†]). After forming the alloys, the proportion of the Pd(II) species increased. The Co 2p spectrum (Fig. S8, ESI[†]) showed that Co exists in the form of Co(II)²⁰ and Co(III).²¹ Thus, the CoPd alloys on NiAl-LDH were in an oxidation state. These results were also in accordance with previously reported loaded CoPd alloys.²⁰

The spectra of the other elements listed in Fig. S10, (ESI[†]) showed no evident differences, indicating the structural similarity.

Whereafter, their CO₂ photoreduction activity was evaluated. The test was conducted under visible light ($\lambda > 420$ nm) with the assistant of [Ru(bpy)₃]Cl₂·6H₂O as a photosensitizer and triethanolamine (TEOA) as a sacrificial agent. Fig. 2a summarizes the production rates of H₂, CO, and CH₄ using different catalysts. When no catalyst was added, the minor amount of H₂ and CO came from the presence of [Ru(bpy)₃]Cl₂·6H₂O.⁷ NiAl-LDH showed the lowest H₂ evolution activity of 38.7 $\mu\text{mol g}^{-1} \text{h}^{-1}$ and a moderate CO evolution rate of 275.0 $\mu\text{mol g}^{-1} \text{h}^{-1}$. Besides, minor amounts of CH₄ were also formed with a production rate of 6.5 $\mu\text{mol g}^{-1} \text{h}^{-1}$. NiAl-LDH-Pd presented a promoted H₂ evolution rate of 169.2 $\mu\text{mol g}^{-1} \text{h}^{-1}$. However, the CO production rate decreased to 102.7 $\mu\text{mol g}^{-1} \text{h}^{-1}$. When the CoPd alloys were loaded, NiAl-LDH-CoPd realized simultaneous improvement of the H₂ and CO production rates, with a 14.5-fold improvement in the H₂ evolution rate and a 2.1-fold improvement in the CO evolution rate compared with NiAl-LDH. Meanwhile, the H₂ and CO production rates were 3.3 times and 5.6 times higher than those of NiAl-LDH-Pd, respectively. Most important of all, the H₂ evolution rate was 563.1 $\mu\text{mol g}^{-1} \text{h}^{-1}$, the CO evolution rate was 570.7 $\mu\text{mol g}^{-1} \text{h}^{-1}$, and the ratio of H₂/CO was very close to 1 : 1, which is an applicable ratio for industrial synthesis. After analyzing the liquid phase reactant with ¹H nuclear magnetic resonance (NMR) spectroscopy (Fig. S11, ESI[†]), no other liquid products were discovered.²² Besides, only a trace amount of CH₄ was detected in NiAl-LDH-Pd and even less in NiAl-LDH-CoPd meaning the CO selectivity was promoted in the carbonaceous products. Then CO₂ was replaced with Ar as the control experiment, and no CO was detected (Fig. 2b), which excluded the influence of contaminants on the photocatalytic performance. In summary, alloying Pd with Co not only improved the photocatalytic activity and selectivity but also realized the formation of syngas with an applicable ratio. The maximum apparent quantum yield (AQY) values were 0.097% for CO production and 0.102% for H₂ production under 475 nm (Table S2, ESI[†]) in NiAl-LDH-CoPd. The XRD patterns (Fig. S12, ESI[†]) and TEM images (Fig. S13, ESI[†]) of the photocatalysts after the reactions reveal the structural stability of the samples.

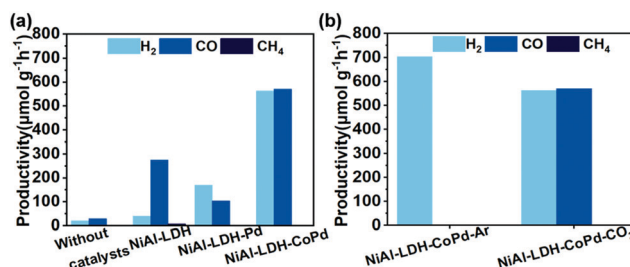


Fig. 2 (a) The yield of H₂, CO, and CH₄ in the photocatalytic CO₂ reduction with different samples; (b) the yield of H₂, CO, and CH₄ using NiAl-LDH-CoPd under Ar and CO₂, respectively (reaction conditions: photosensitizer: 2 μmol [Ru(bpy)₃]Cl₂·6H₂O; photocatalyst: 1 mg mL⁻¹; solvent: 5 mL (CH₃CN/TEOA/H₂O = 3/1/1 (v/v/v)); 1 h).

To explore the activity stability, a recycling test was conducted (Fig. S14, ESI[†]). The NiAl-LDH-CoPd still presented a nearly 1:1 ratio of H₂ and CO in the third experiment, and the yields of H₂ and CO were 73% and 81% of the original production rates, respectively.

To understand the role of the alloys in promoting the photocatalytic activity, we investigated the charge kinetics. Fig. S15 (ESI[†]) displays the UV-visible diffuse reflectance spectra (UV-vis) of the catalysts. All the samples responded to visible light, and both the loading of Pd and CoPd nanoparticles improved the absorbability of light. Although NiAl-LDH-Pd showed the strongest absorbability, NiAl-LDH-CoPd presented the highest photocurrent response (Fig. 3a), which was about 3 and 2 times higher than those of NiAl-LDH and NiAl-LDH-Pd, respectively. This indicated that loading Pd nanoparticles can promote the separation and transfer of photogenerated charge carriers while alloying Pd with Co will further enhance it.²³ Although it was not reliable to compare the recombination possibility of NiAl-LDH-Pd and NiAl-LDH-CoPd from the PL spectra (Fig. S16, ESI[†]) due to the weak signal, the spectra still revealed depressed charge carriers recombination of the two compared with NiAl-LDH. Additionally, we carried out Mott-Schottky tests. In Fig. S17 (ESI[†]), NiAl-LDH-CoPd showed the smallest slope of the Mott-Schottky plot, and NiAl-LDH showed the largest. Therefore, charge carrier transfer was most favorable over NiAl-LDH-CoPd and least favorable over NiAl-LDH.²⁴ Accordingly, the CoPd alloys played a vital role in facilitating the separation and transfer of charge carriers. Principally, the loaded metal nanoparticles with larger work functions can form Schottky junctions with the semiconductors with smaller work functions, in which the charge transfers from

the semiconductors to the metals until the Fermi levels are aligned. The Schottky junction can promote charge separation. The XPS valence band spectra (Fig. 3b) showed that NiAl-LDH-CoPd and NiAl-LDH-Pd both exhibited values with lower binding energies compared with NiAl-LDH, which confirmed the charge transfer from NiAl-LDH to the loaded metals and the formation of the Schottky junction,²⁵ thus explaining their promoted charge kinetics compared to NiAl-LDH. The Schottky barrier height is the difference between the electron affinity of NiAl-LDH and the work functions of the loaded metals.¹⁵ As shown in Fig. 3c and d, the work function of Co (5.00 eV) is smaller than that of Pd (5.55 eV),²⁶ and alloying Pd with Co will decrease the work function and lower the height of the Schottky barrier.^{15,25} In NiAl-LDH-Pd, the larger Schottky barrier height can promote charge carrier separation, but at the same time it may suppress the transfer of electrons from NiAl-LDH to Pd.^{15,27} While in NiAl-LDH-CoPd, the smaller Schottky barrier height may be more appropriate for smooth electron transfer from NiAl-LDH to CoPd when facilitating the separation of charge carriers. This may explain the best charge separation and transfer behaviour in NiAl-LDH-CoPd.

The adsorption of reactants is also a critical step in photocatalytic reactions. To gain a profound insight into the reasons for the better photocatalytic performance of NiAl-LDH-CoPd than that of NiAl-LDH-Pd, we carried out DFT calculations of the adsorption energies (E_{ads}) for CO₂ and H₂O on the surfaces of the two. As the optimized configurations showed, the active sites for CO₂ adsorption in NiAl-LDH-Pd were Pd atoms, and showed an E_{ads} of -0.75 eV (Fig. 4a). After alloying Pd with Co, the active sites were regulated to the paired Pd-Co atoms with an E_{ads} of -1.43 eV (Fig. 4b), thus promoting the adsorption and activation of CO₂ and contributing to the improved CO yield. Besides, the Co atoms in NiAl-LDH-CoPd (Fig. 4d) presented an obviously stronger H₂O affinity (E_{ads} = -1.19 eV) than that of the Pd atoms (Fig. 4c) in NiAl-LDH-Pd (E_{ads} = -0.36 eV), which meant H₂ evolution was easier in NiAl-LDH-CoPd than that in NiAl-LDH-Pd.⁹ Thus, alloying Pd with Co modified the active sites to be more appropriate for both H₂ evolution and CO₂ photocatalytic reduction, and enhance the productivity of syngas.

Pd possesses a lower overpotential for H₂ evolution.⁹ Besides, the loading of Pd nanoparticles enhanced the separation and transfer of charge carriers. Thus, NiAl-LDH-Pd showed an increased H₂ evolution rate compared with NiAl-LDH. However, the CO evolution is not improved. Co is a widely reported active site in photocatalytic CO₂ reduction.^{6,28} After alloying Pd with Co, the H₂O and CO₂ affinity improved simultaneously. What's more, the ability for charge transfer was further increased. Hence, NiAl-LDH-CoPd presented a promoted photocatalytic performance for both H₂ and CO evolution. The possible photocatalytic process of NiAl-LDH-CoPd is illustrated in Fig. S16 (ESI[†]). [Ru(bpy)₃]Cl₂·6H₂O was first excited to generate photoelectrons and became [Ru(bpy)₃]³⁺. Then the photoelectrons transferred to NiAl-LDH-CoPd, and reduced H⁺ to active hydrogen species (H*) atoms. The H* atoms combined with the CO₂ on the surface of the photocatalyst to

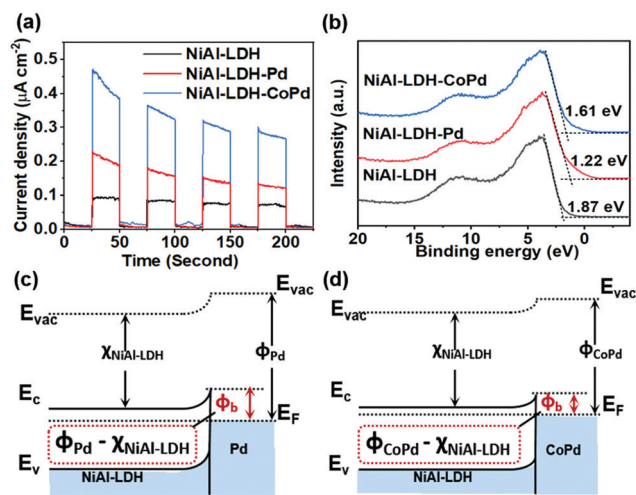


Fig. 3 (a) Photocurrent vs. time ($I-t$) curves at 0.28 V vs. Ag/AgCl for NiAl-LDH, NiAl-LDH-Pd, and NiAl-LDH-CoPd under UV-visible light irradiation; (b) valence-band XPS spectra of NiAl-LDH, NiAl-LDH-Pd, and NiAl-LDH-CoPd; schematic energy-band diagrams for (c) NiAl-LDH-Pd, and (d) NiAl-LDH-CoPd. E_{vac} , E_{v} , E_{c} , E_{F} , Φ_{b} , Φ_{Pd} , Φ_{CoPd} , and $\chi_{\text{NiAl-LDH}}$ denote the vacuum level, the conduction band, the valence band, the Fermi level, the Schottky barrier height, the work function of Pd, the work function of CoPd, and the electron affinity of the NiAl-LDH conduction band, respectively (in eV).

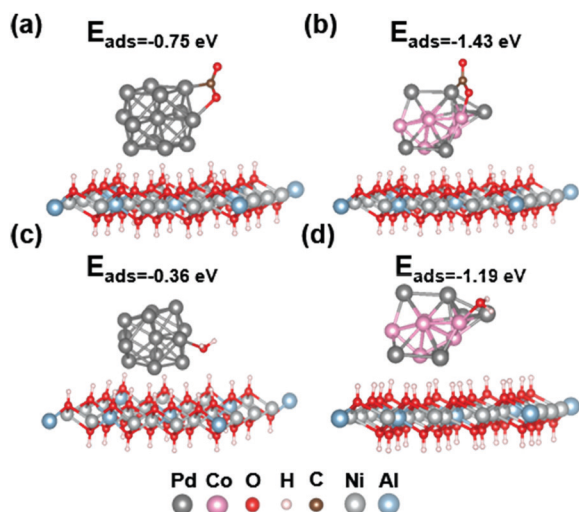


Fig. 4 Optimised configurations and adsorption energies of CO₂ at (a) NiAl-LDH-Pd, and (b) NiAl-LDH-CoPd; optimised configurations and adsorption energies of H₂O at (c) NiAl-LDH-Pd, and (d) NiAl-LDH-CoPd.

subsequently yield CO. Meanwhile, the H* atoms combine to produce H₂ and [Ru(bpy)₃]³⁺ is recovered to [Ru(bpy)₃]²⁺ by the reduction of TEOA.^{7,9}

In summary, *via* loading CoPd alloys, we prepared a NiAl-LDH-CoPd photocatalyst fulfilling the promotion of the photocatalytic reduction of CO₂ and generating syngas under visible light. The CoPd alloys can facilitate the separation and transfer of charge carriers, and optimize adsorption and activation to CO₂ and H₂O simultaneously, leading to the promotion of photocatalytic activity for syngas production. This work may provide a potential strategy to design photocatalysts with similar structures for syngas production. We will work on the regulation of syngas ratio and yields by alloying different amounts and kinds of metals in the future.

This work was financially supported by the Strategic Priority Research Program of the Chinese Academy of Sciences (XDB36030300), the National Natural Science Foundation of China (21890754), the National Natural Science Foundation of China National Key R&D Program of China (2017YFA0207301 and 2017YFA0303500), the Youth Innovation Promotion Association CAS (Y202092), and the Fundamental Research Funds for the Central University (WK2340000094).

Conflicts of interest

There are no conflicts to declare.

Notes and references

- 1 K. Cheng, B. Gu, X. Liu, J. Kang, Q. Zhang and Y. Wang, *Angew. Chem., Int. Ed.*, 2016, **55**, 4725–4728.
- 2 S. Chu, S. Fan, Y. Wang, D. Rossouw, Y. Wang, G. A. Botton and Z. Mi, *Angew. Chem., Int. Ed.*, 2016, **55**, 14262–14266.
- 3 S. R. Foit, I. C. Vinke, L. G. J. de Haart and R.-A. Eichel, *Angew. Chem., Int. Ed.*, 2017, **56**, 5402–5411.
- 4 A. Li, T. Wang, X. Chang, Z. J. Zhao, C. Li, Z. Huang, P. Yang, G. Zhou and J. Gong, *Chem. Sci.*, 2018, **9**, 5334–5340.
- 5 D. Li, S. Ouyang, H. Xu, D. Lu, M. Zhao, X. Zhang and J. Ye, *Chem. Commun.*, 2016, **52**, 5989–5992.
- 6 S. Wang, W. Yao, J. Lin, Z. Ding and X. Wang, *Angew. Chem., Int. Ed.*, 2014, **53**, 1034–1038.
- 7 C. Qiu, X. Hao, L. Tan, X. Wang, W. Cao, J. Liu, Y. Zhao and Y. F. Song, *Chem. Commun.*, 2020, **56**, 5354–5357.
- 8 C. Ning, Z. Wang, S. Bai, L. Tan, H. Dong, Y. Xu, X. Hao, T. Shen, J. Zhao, P. Zhao, Z. Li, Y. Zhao and Y.-F. Song, *Chem. Eng. J.*, 2021, **412**, 128362.
- 9 X. Wang, Z. Wang, Y. Bai, L. Tan, Y. Xu, X. Hao, J. Wang, A. H. Mahadi, Y. Zhao, L. Zheng and Y.-F. Song, *J. Energy Chem.*, 2020, **46**, 1–7.
- 10 N. Ahmed, Y. Shibata, T. Taniguchi and Y. Izumi, *J. Catal.*, 2011, **279**, 123–135.
- 11 H. Jiang, K.-i. Katsumata, J. Hong, A. Yamaguchi, K. Nakata, C. Terashima, N. Matsushita, M. Miyauchi and A. Fujishima, *Appl. Catal., B*, 2018, **224**, 783–790.
- 12 Y. F. Zhao, X. D. Jia, G. I. N. Waterhouse, L. Z. Wu, C. H. Tung, D. O'Hare and T. R. Zhang, *Adv. Energy Mater.*, 2016, **6**, 1501974.
- 13 R. Long, Y. Li, Y. Liu, S. Chen, X. Zheng, C. Gao, C. He, N. Chen, Z. Qi, L. Song, J. Jiang, J. Zhu and Y. Xiong, *J. Am. Chem. Soc.*, 2017, **139**, 4486–4492.
- 14 J. Zhang, Y. Lu, L. Ge, C. Han, Y. Li, Y. Gao, S. Li and H. Xu, *Appl. Catal., B*, 2017, **204**, 385–393.
- 15 D. Tsukamoto, A. Shiro, Y. Shiraishi, Y. Sugano, S. Ichikawa, S. Tanaka and T. Hirai, *ACS Catal.*, 2012, **2**, 599–603.
- 16 N. Iyi, Y. Ebina and T. Sasaki, *J. Mater. Chem.*, 2011, **21**, 8085–8095.
- 17 W. Wang, N. Zhang, Z. Shi, Z. Ye, Q. Gao, M. Zhi and Z. Hong, *Chem. Eng. J.*, 2018, **338**, 55–61.
- 18 P. Li, W. Liu, J. S. Dennis and H. C. Zeng, *Adv. Funct. Mater.*, 2016, **26**, 5658–5668.
- 19 S. F. Ho, A. Mendoza-Garcia, S. Guo, K. He, D. Su, S. Liu, O. Metin and S. Sun, *Nanoscale*, 2014, **6**, 6970–6973.
- 20 H.-J. Oh, V.-D. Dao and H.-S. Choi, *J. Alloys Compd.*, 2017, **705**, 610–617.
- 21 B. J. Tan, K. J. Klabunde and P. M. Sherwood, *J. Am. Chem. Soc.*, 1991, **113**, 855–861.
- 22 L. Tan, S. M. Xu, Z. Wang, Y. Xu, X. Wang, X. Hao, S. Bai, C. Ning, Y. Wang, W. Zhang, Y. K. Jo, S. J. Hwang, X. Cao, X. Zheng, H. Yan, Y. Zhao, H. Duan and Y. F. Song, *Angew. Chem., Int. Ed.*, 2019, **58**, 11860–11867.
- 23 K. Zhang, Y. Liu, J. Deng, S. Xie, X. Zhao, J. Yang, Z. Han and H. Dai, *Appl. Catal., B*, 2018, **224**, 350–359.
- 24 F. Su, T. Wang, R. Lv, J. Zhang, P. Zhang, J. Lu and J. Gong, *Nanoscale*, 2013, **5**, 9001–9009.
- 25 Q. Liu, Q. Chen, T. Li, Q. Ren, S. Zhong, Y. Zhao and S. Bai, *J. Mater. Chem. A*, 2019, **7**, 27007–27015.
- 26 D. Eastman, *Phys. Rev. B: Solid State*, 1970, **2**, 1.
- 27 T. Uchihara, M. Matsumura, A. Yamamoto and H. Tsubomura, *J. Phys. Chem. C*, 1989, **93**, 5870–5874.
- 28 Q. Mu, W. Zhu, G. Yan, Y. Lian, Y. Yao, Q. Li, Y. Tian, P. Zhang, Z. Deng and Y. Peng, *J. Mater. Chem. A*, 2018, **6**, 21110–21119.